Protein-Directed Synthesis of NIR-Emitting, Tunable HgS Quantum Dots and their Applications in Metal-Ion Sensing

Nirmal Goswami, Anupam Giri, Shantimoy Kar,
Megalamane Siddaramappa Bootharaju, Robin John,
Paulrajpillai Lourdu Xavier, Thalappil Pradeep,* and Samir Kumar Pal*

The development of luminescent mercury sulfide quantum dots (HgS QDs) through the bio-mineralization process has remained unexplored. Herein, a simple, two-step route for the synthesis of HgS quantum dots in bovine serum albumin (BSA) is reported. The QDs are characterized by UV–vis spectroscopy, Fourier transform infrared (FT-IR) spectroscopy, luminescence, Raman spectroscopy, transmission electron microscopy (TEM), X-ray photoelectron spectroscopy (XPS), circular dichroism (CD), energy dispersive X-ray analysis (EDX), and picosecond-resolved optical spectroscopy. Formation of various sizes of QDs is observed by modifying the conditions suitably. The QDs also show tunable luminescence over the 680–800 nm spectral regions, with a quantum yield of 4–5%. The as-prepared QDs can serve as selective sensor materials for Hg(II) and Cu(II), based on selective luminescence quenching. The quenching mechanism is found to be based on Dexter energy transfer and photoinduced electron transfer for Hg(II) and Cu(II), respectively. The simple synthesis route of protein-capped HgS QDs would provide additional impetus to explore applications for these materials.

1. Introduction

In the past decade, semiconductor quantum dots (QDs) have become well-established photoluminescent platforms for many scientific and industrial applications.[1–3] For example, QDs are highly sensitive to charge/energy transfer, which can alter their optical properties, thus generating interest in charge/energy-transfer-based bio-sensing.[1,4] Among all the semiconducting QDs, mercury chalcogenide QDs are one of the least studied families because of the toxicity and volatility of corresponding organo-mercury compounds. Such materials are highly attractive for infrared sensing, optoelectronics, as well as for the more fundamental studies of their optical properties. Luminescence across the visible spectral region with mercury chalcogenide is extremely difficult, while it is common for zinc- and cadmium-based chalcogenides. Despite the potential toxicity of mercury and the restricted application in biology, it would be of great interest to develop

N. Goswami, A. Giri, S. Kar, Dr. S. K. Pal
Department of Chemical
Biological & Macromolecular Sciences
S. N. Bose National Centre for Basic Sciences
Block JD, Sector III, Salt Lake, Kolkata 700 098, India
E-mail: skpal@bose.res.in

M. S. Bootharaju, R. John, P. L. Xavier, Prof. T. Pradeep
Department of Chemistry
Indian Institute of Technology Madras
Chennai 600 036, India
E-mail: pradeep@iitm.ac.in

mercury chalcogenide QDs with tunable luminescence as there is immense potentiality in their application in chemical sensing, infrared detection, and in the development of electrical devices.[2,5,6]

Of all the mercury chalcogenides, HgTe is widely studied, having various synthetic routes leading to high-quality materials based on both aqueous- and organic-based chemistries. Recently, Keuleyan et al.[7] prepared colloidal HgTe QDs having narrow photoluminescence tunable across the near and mid-IR regions. In contrast, there have been very few detailed studies on HgS QDs. Wichiansee et al.[8] have successfully prepared HgS QDs based on an organic route, using trioctylphosphine oxide (TOPO) as the capping agent. Higginson et al.[9] have synthesized HgS QDs exhibiting narrow, size-dependent transitions between 500 and 800 nm for sizes ranging from 1 to 5 nm in diameter. Typically, in most cases, HgS QDs were synthesized via thermal decomposition of organo-metallic precursors in organic solvents and/or in the presence of surfactants.[8,10,11] However, unlike them, the use of a biomolecule as template or scaffold for the synthesis possesses many advantages due to their inherent biocompatibility and ease of functionalization. Thus, novel synthetic strategies for the preparation of HgS QDs using biomolecules that yield extremely stable, water-soluble QDs with tunable luminescence in the visible and near IR (NIR) region would be highly desirable.

Among many biological systems that could participate in biomineralization and be incorporated into bio-nanomaterials, proteins have been the subject of particular attention due to their nanoscale dimensions, distinctive molecular structures and functionalities, and their capability to control the size of inorganic crystals during nucleation and growth to a remarkable degree due to their bulky nature. For example, bovine serum albumin (BSA) and several other proteins have been used to synthesize sub-nanometer luminescent metal clusters.[12–18] Recently, an aqueous, protein-driven synthesis of transition-metal-doped ZnS QDs has also been reported by Zhou et al.[19] Akin to the bio-mineralization process, herein, we have developed a facile approach to prepare water-soluble, highly stable NIR-luminescent HgS QDs, which are protected and stabilized by the protein matrix. We have also used the HgS QDs formed as a fluorometric sensor for the detection of Hg(II) and Cu(II). Uses of the QDs in metal-ion sensing by exploiting their luminescence properties is not new and have been reported before.[20,21] The mechanisms of luminescence quenching involving inner-filter effects, nonradiative recombination pathways, and electron transfer processes have also been reported. However, the quenching mechanisms addressing the specific interaction of detected ions with the sensor QDs are sparse in the existing literature. The reason for quenching relies on the metallophilic interaction between Hg(II)/Cu(II) and Hg(II) present
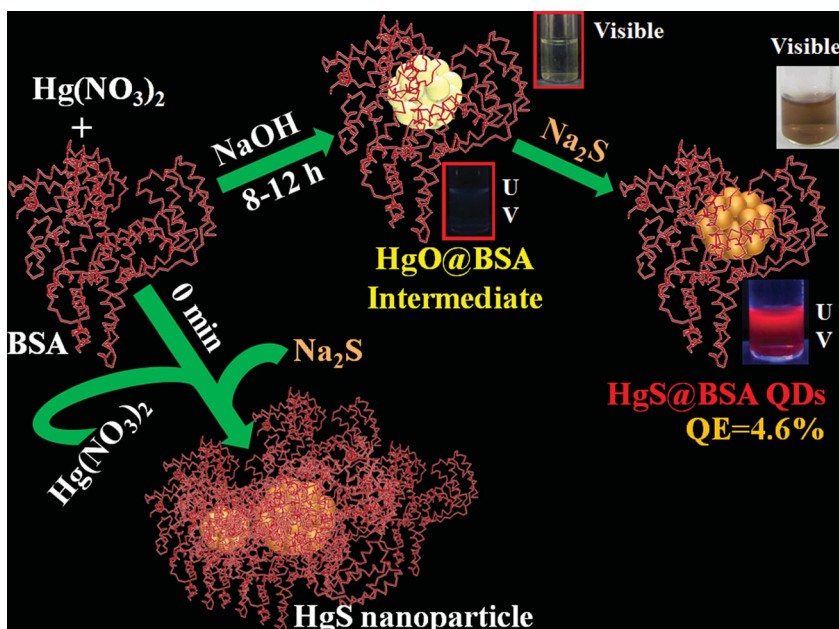
Scheme 1. Schematic illustration of the synthesis of HgS QDs through the bio-mineralization process mediated by the BSA protein.

on the surface of the HgS QDs. We have used time-resolved luminescence methods to study the mechanism of excited-state reactivity, which reveals that both Hg(II) and Cu(II) can reduce the lifetime of the HgS QDs. After considering all kinds of excited-state deactivation mechanisms, we have found that Dexter energy transfer is the reason in the case of Hg(II)-induced quenching whereas photoinduced electron transfer dominates in the case of Cu(II)-induced quenching. In several control experiments, we have also ruled out other possibilities for the quenching mechanisms, including aggregation and Förster resonance energy transfer (FRET).

2. Results and Discussion

The process for synthesizing the HgS QDs is simple and involves two steps (see Experimental Section for details). The various stages of synthesis are shown in **Scheme 1**. In the first step, addition of mercury nitrate solution to aqueous BSA causes the mercury ions to be coordinated with the various functional groups of BSA such as –SH and –NH. The pH of the solution was adjusted to ~9 by the addition of NaOH followed by vigorous stirring at room temperature. After 8–12 h, the color of the solution changes from colorless to a pale yellow intermediate, which we have analyzed by Raman spectroscopy (see later in text) and found it to be HgO@BSA. Photographs of the intermediate under UV and visible light are shown in Scheme 1. In the last step, Na₂S is added and the color changes from pale yellow to light brown (Scheme 1), which indicates the formation of HgS QDs. **Figure 1**A illustrates the UV–vis absorption spectra of HgS@BSA QDs. In particular, Figure 1A gives the plot of the natural logarithm of the Jacobian factor (details in Experimental Section) versus wavelength of the QDs, to show the features more clearly. Well-defined absorption
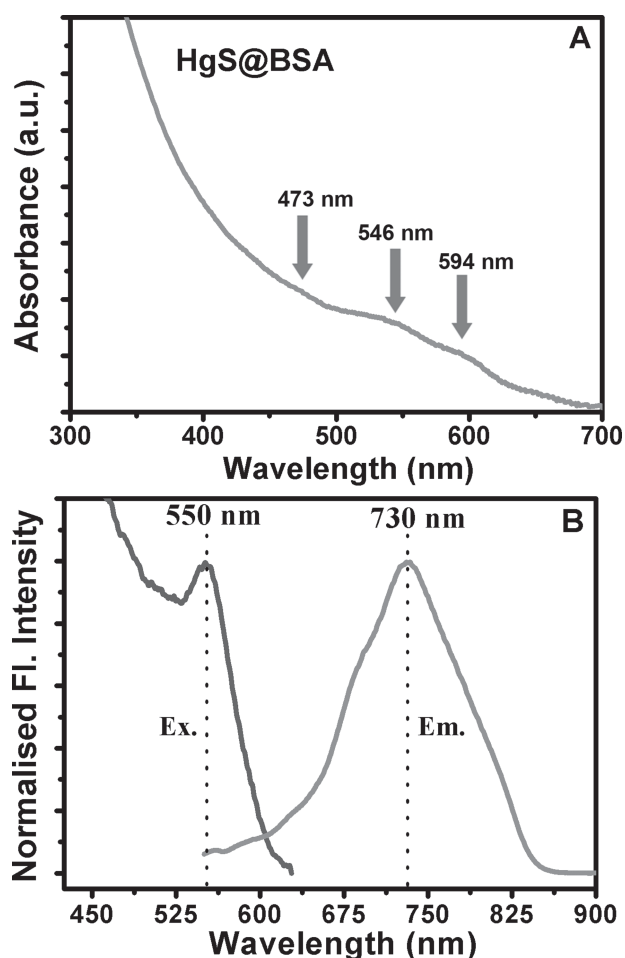
Figure 1. A) UV-Vis absorbance spectrum of HgS@BSA. B) Excitation and emission spectrum of HgS@BSA. Excitation spectrum is taken by monitoring at 730 nm. Luminescence spectrum is collected with 450 nm excitation.

UV and visible radiations are shown in Scheme 1. As a control study, we have performed the reaction in the absence of Na_2S; however, no such luminescent material is obtained even after 48 h (Figure S2, SI). This result reveals that external sulphur is required for the growth of QDs. It has to be noted that direct addition of mercury nitrate and Na_2S with protein solution leads to the formation of nonluminescent HgS nanomaterial, which provides evidence that the formation of the yellow intermediate is necessary to obtain the luminescent QDs (Figure S3, SI). The photoluminescence quantum yield of the HgS@BSA is ~4.6%, estimated using 4-(dicyanomethylene)-2-methyl-6-(*p*-dimethylaminostyryl)-4H-pyran (DCM) as a reference with a 450 nm excitation wavelength. The obtained HgS QDs are found to be very stable, showing the same luminescence spectra after almost seven days of being stored at room temperature (Figure S4, SI). The luminescence is maximum at neutral pH, however, relatively less stable in acidic and basic pH as shown in Figure S5 (SI). In order to investigate the thermal stability of the QDs, temperature-dependent luminescence of HgS@ BSA has been monitored. It can be seen from Figure S6 (SI) that luminescence of the HgS@BSA in the aqueous solution decreased significantly upon increase in temperature. The reason may be the increase in hydrophilicity around the HgS QDs as protein is perturbed at higher temperature.

By varying the experimental conditions, e.g., Hg/S ratio, we achieved variations in the diameter of the QDs, resulting in the tunability of their luminescence (**Figure 2**A). As shown in Figure 2B, a variation of excitation peak maxima is clearly observed, pointing to the presence of QDs having different sizes. In the photoluminescence spectra the peak maxima varied from 680 to 800 nm, which corresponds to a QD diameter varying from 4 to 10 nm according to our dynamic light scattering (DLS) results (Figure 2C).

A high-resolution transmission electrom microscopy (HR-TEM) image confirmed the presence of nearly spherical
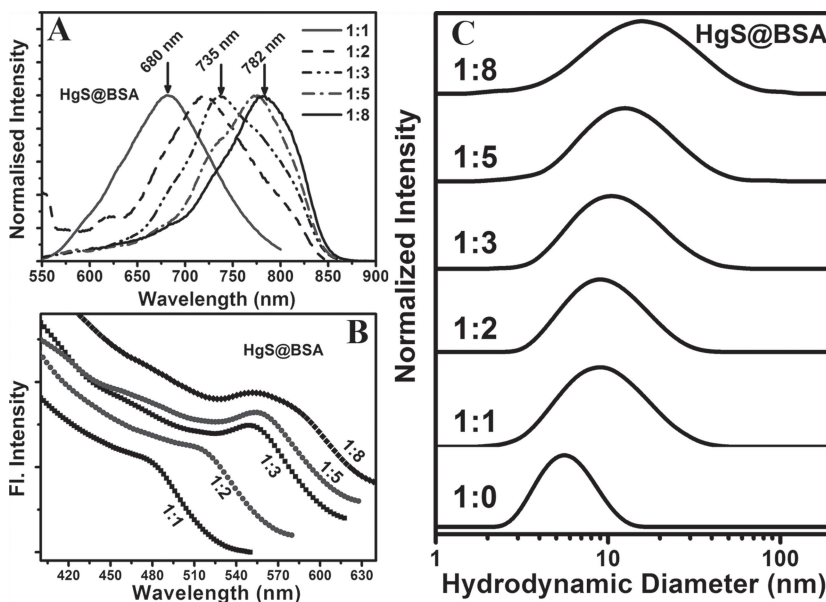
features are marked with arrows. Three distinct excitonic absorption shoulders of the HgS QDs are found at 473 (2.62), 546 (2.27), and 594 nm (2.09 eV), which indicate the presence of differently sized QDs. The bandgaps calculated for UV features at 2.62, 2.27, and 2.09 eV are 2.02, 1.94 and 1.90 eV, respectively, which are very much blue-shifted from the average bandgap of bulk *β*-HgS (–0.2 to 0.5 eV)[8] due to a high quantum confinement effect. Figure 1B shows the luminescence profile of the as-prepared QDs. A clear excitation maximum at 550 nm and a luminescence peak at around 730 nm is evident from Figure 1B. Note that, similar to the absorption spectrum, the luminescence spectrum is also broad and can be fitted into three different peaks having maxima at 680 (1.82), 733 (1.69), and 803 nm (1.54 eV) (Figure S1, Supporting Information (SI)). Photographs of QDs under

Figure 2. Normalized spectra. A). Luminescence, B) excitation, and C) dynamic light scattering spectra for HgS@BSA QDs with different Hg/S molar ratios.
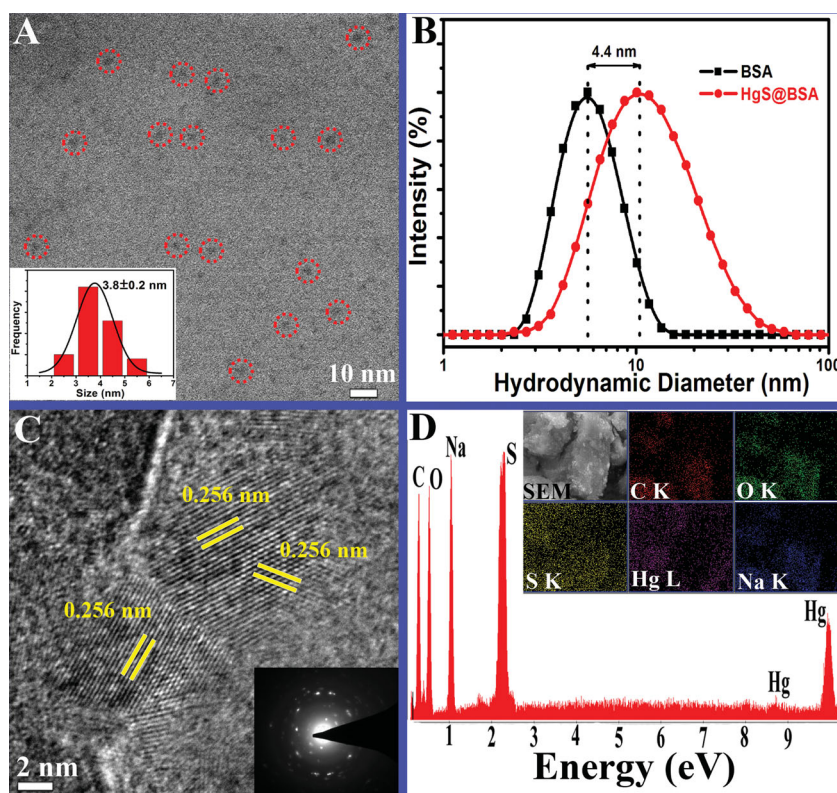
Figure 3. A) Typical TEM images of HgS QDs. The size distribution of HgS@BSA is shown in the inset. B) Dynamic light scattering spectra of BSA and HgS@BSA in aquous solution at pH ~9. The swelling of the protein size by 4.4 nm has also been assigned. C) High-resolution TEM image of HgS QDs. SAED pattern in an area including HgS QDs is shown in the inset. D) EDX spectrum collected for HgS@BSA. Inset showing the SEM image of the HgS@BSA sample from which the EDX spectrum was taken. EDX maps obtained using the C K, O K, S K, Hg L, and Na K lines are also shown in the inset.

nanocrystals having a size of 3.8 ± 0.2 nm (**Figure 3**A). As shown in Figure 3B, the characteristic hydrodynamic diameter of BSA is shifted from 5.6(±0.6) nm to 9.3(±0.6) nm accroding to DLS after the formation of HgS QDs. This observation is consistent with the fact that QDs are formed within the protein matrix. Again, the size obtained from the TEM study is roughly comparable to the swelling of the protein size (~4.4 ± 0.6 nm), as revealed from our DLS measurements. The HR-TEM image of the HgS QDs is shown in Figure 3C. The distance between two adjacent planes is 0.29 nm, corresponding to the (200) lattice plane of cubic β-HgS (International Centre for Diffraction Data (ICDD), Reference no: 00-002-0453). The distinct fringe spacing and the corresponding selected-area electron diffraction (SAED) pattern (inset of Figure 3C) reveal the reasonably good crystallinity of the as-prepared HgS QDs. Moreover, the elemental composition of the HgS QDs is confirmed from X-ray diffraction (XRD) data (Figure S7, SI), energy dispersive X-ray analysis (EDX), and elemental mapping of the scanning electron microscopy (SEM) image. Figure 3D demonstrates the EDX spectrum of the HgS@BSA. SEM image of the HgS@BSA and EDX maps using the C K, O K, S K, Hg L, and Na K lines are shown in the inset of Figure 3D.

X-ray photoelectron spectroscopy (XPS) of the intermediate, HgO@BSA, and the final product, HgS@BSA, were

carried out to verify the oxidation state of Hg and the elemental composition. Survey spectra of HgO@BSA and HgS@BSA show the expected elements, C, N, O, S (from protein and QDs), and Hg (from QDs) (Figure S8, SI). The Hg 4f regions of the above samples are compared with the synthesized bulk HgO and HgS in **Figure 4**. The Hg $4f_{7/2}$ peaks of bulk HgO and HgS appeared at 100.6 and 100.1 eV, respectively, whereas in HgO@BSA and HgS@BSA, they are at 101.4 and 100.6 eV, respectively. These higher-energy peaks in the nanoparticles confirms the presence of mercury in +2 state in all the samples. The shift of the Hg $4f_{7/2}$ peak to a higher binding energy in both HgO@BSA and HgS@BSA samples indicate the functionalization of HgO and HgS by protein and the difference from the corresponding bulk systems. The presence of S $2p_{3/2}$ in bulk HgS, which results in peaks at 161.2 and 168.0 eV, is due to sulphide and partially oxidized species, such as sulphate, respectively (Figure S9A, SI). The formation of HgS in the protein sample was confirmed by the presence of S $2p_{3/2}$ around 161.2 eV (Figure S9B, trace b, SI). The presence of other sulphur species such as disulphides and sulphates (due to X-ray induced damage which is expected in protein samples)[16] are observed in the HgO@BSA and HgS@BSA samples (S $2p_{3/2}$ peaks at 163.3 and 167.8 eV).

Raman spectroscopic measurements were performed on the HgS QDs formed and the reaction intermediate to elucidate the reaction mechanism. The spectra of bulk HgO, bulk HgS, HgO@BSA, HgS@BSA, and BSA are compared in **Figure 5**A. Bulk HgO has a main band centered at 334 cm^{-1} whereas the intermediate has a red-shifted feature at 330 cm^{-1}; which originates from the oxygen interchain mode of the HgO with A_g symmetry.[22] These features are highlighted using a dotted circle in Figure 5A. The Raman spectrum of the HgS QDs shows a slightly blue-shifted peak around 262 cm^{-1}, in comparison to bulk HgS which has a feature at 254 cm^{-1} (dashed circle) originating from a mode of A_1 symmetry.[23] BSA has several Raman features corresponding to the detailed structure of the protein including the amide signatures as given in Table S1 (SI).[24] It should be noted that several of these features are retained in the Raman spectra of the reaction intermediate and the QDs, confirming the formation of HgO and HgS, respectively, in the protein. In the case of HgO@BSA, the amide regions of the protein are more distorted (or several features could be merged) than in the case of HgS@BSA.

Fourier Transform infrared (FT-IR) spectroscopy has been one of the most common methods to investigate the structure of proteins by probing their functional group signatures. Amide I, II, and III bands provide information about
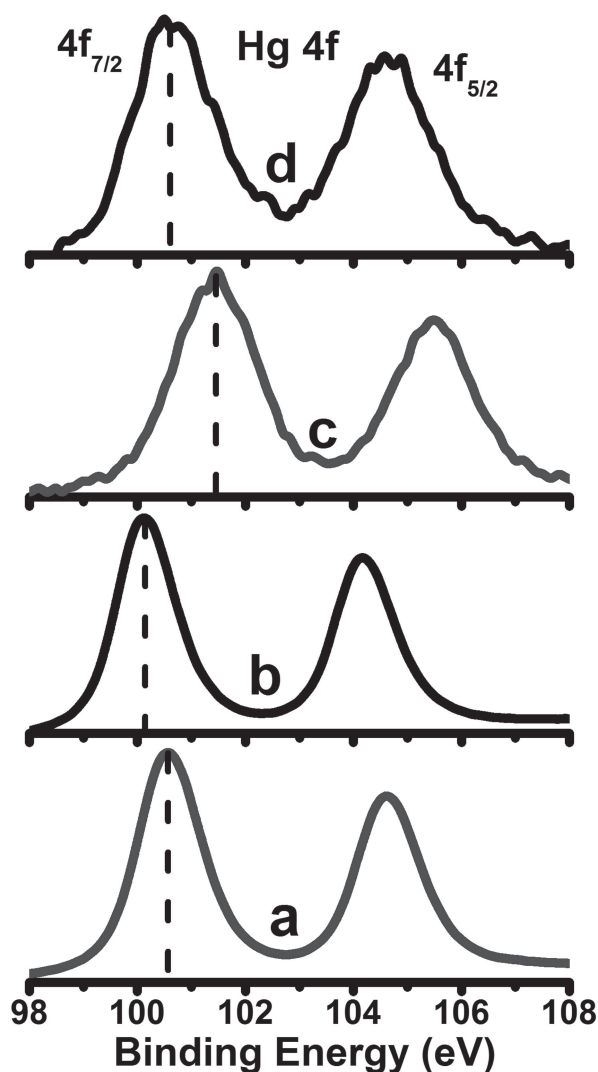
Figure 4. XPS spectra in the Hg 4f region of a) bulk HgO, b) bulk HgS, c) HgO@BSA, and d) HgS@BSA. The vertical dotted lines represent the Hg $4f_{7/2}$ binding energies.

the secondary structural changes in proteins.[25–27] Solid-state IR analysis results suggested, in general, that the bands were broadened and shifted to a higher frequency, indicating perturbation of the secondary structure. Spectral regions within or near 1600–1690, 1480–1575, 1229–1301, and 3300 cm^{-1} have been assigned as amide I, amide II, amide III, and amide A, respectively (Figure 5B). The increase in the intensity and decrease in the peak width is seen around 1399 cm^{-1}, which is attributed to the C=O stretching of COO$^-$, suggests that the COO$^-$ groups are more influenced by the formation of HgO and HgS or could be associated with the Hg in the protein matrix. Regions within 1651–1658, 1618–1642, 1666–1688, and 1650 ± 1 cm^{-1} have been assigned as α-helix, β sheets, turns, and unordered structures, respectively.[27] The band appearing around 700 cm^{-1} can be assigned to –NH$_2$ and –NH wagging, and the band around 2960 cm^{-1} can be attributed to C−H vibrations. The band near 1400 cm^{-1} is due to the C=O stretching of COO$^-$, and that at 1468 cm^{-1} can be assigned as the C−H deformation of >CH2, and that at 3500 cm^{-1} is

due to O−H stretching.[25,27] In the second-derivative spectra, compared to native BSA, in HgO@BSA and HgS@BSA, the α-helix content decreased significantly as indicated by the prominent band at 1655 cm^{-1} disappearing, and the amount of β-turns increased as indicated by the 1662–1688 cm^{-1} region. In case of HgO@BSA, comparatively the β-turn content was higher than in native BSA and HgS@BSA, suggesting more perturbation in the intermediate form. A new band around 1651 cm^{-1} may be attributed to the increased in random coil structures. This observation is coroborated by observation made in Raman measurements.

Circular dichroism (CD) has been employed to study the conformational behavior of BSA before and after the formation of the HgS QDs. Native BSA displays CD features with minima at 208 and 222 nm, corresponding to the secondary structure of the protein (Figure 5C). Figure 5C shows the decrease of molar ellipticity in the presence of Hg(II), which describes more structural perturbation. From Figure 5C, it is also reflected that there is an insignificant perturbation of the secondary structure of the protein after the addition of Na$_2$S. The observation clearly signifies that addition of Na$_2$S has minimal effect on the secondary structure of the protein.

The optical responses of HgS QDs towards metal ions such as Hg(II), Ca(II), Cu(II), Co(II), Zn(II), Ni(II), Cd(II), Mg(II), Na(I), and K(I) have been investigated. Among these ions, only Cu(II) and Hg(II) can quench the luminescence of the as-prepared HgS QDs. **Figure 6** demonstrates the high optical selectivity and sensitivity of the QDs towards Cu(II) and Hg(II) over other biologically relevant metal ions, and can be seen with the naked eye (Figure 6, lower panel). The mechanism to be proposed below is due to the following reasons: A number of sulphur and Hg(II) (having 5d^{10}6s^0 electronic configuration) are present on the surface of the HgS QDs. Addition of metal ions to the HgS QD solution therefore generates two possibilities: either it will interact with sulphur or with mercury. Moreover, sulphur has an affinity towards other metal ions including Hg(II), Cu(II), Zn(II), and Cd(II). Thus, if the quenching of the luminescence of QDs occurs through the interaction with sulphur, then all of the above mentioned metal ions are expected to reduce the luminescence of HgS@BSA. However, the almost insignificant changes in the QDs luminescence spectrum observed with Zn(II) and Cd(II) (Figure 6), clearly rules out the possibility of luminescence quenching through the interaction with sulphur. Recent theoretical studies suggest that metal centres with a d^{10} electronic configuration have a strong affinity towards other closed-shell metal ions with similar electronic configuration.[28] In particular, this phenomenon associated with strong d^{10}–d^{10} interactions is known as metallophilic interaction.[29] This interaction originates due to dispersive forces which are further augmented by relativistic effects.[29] In the case of the mercury ion (5d^{10}6s^0), a number of examples of such interactions are present in the literature, even in the absence of protecting ligands.[13,14,30] Our study suggests that luminescence quenching of HgS QDs in the presence of Hg(II) is due to the same 5d^{10}–5d^{10} metallophilic interaction (**Scheme 2**). In the case of Cu(II), luminescence quenching could occur through the 5d^{10}–3d^{10} metallophilic interaction
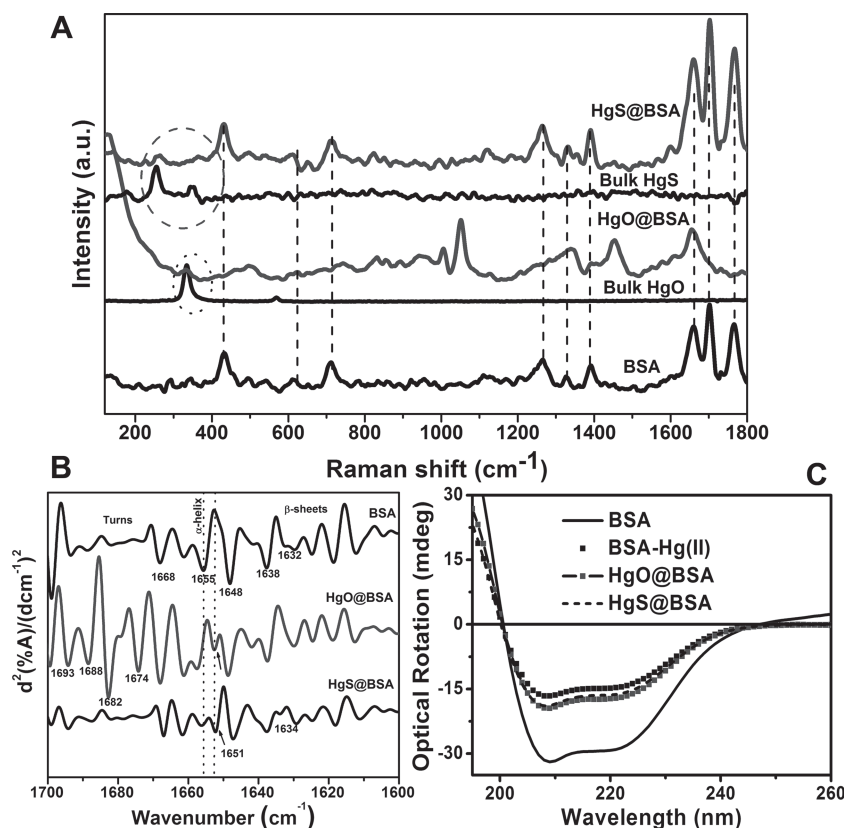
Figure 5. A) Raman spectra of BSA, bulk HgO, HgO@BSA, bulk HgS, and HgS@BSA in solid state collected using a 633 HeNe laser. The dotted marking highlights the presence of features due to A_g oxygen interchain mode in HgO and HgO@BSA as well. The dashed marking highlights the presence of HgS vibrations (A_1 mode of the sulfur atom in HgS) in the NIR-emitting HgQD, confirming the product to be HgS@BSA. B) Second-derivative spectra of amide I region of BSA, HgO@BSA, and HgS@BSA. C) Circular dichroism spectra of BSA, BSA-Hg(II) complex, HgO@BSA, and HgS@BSA.
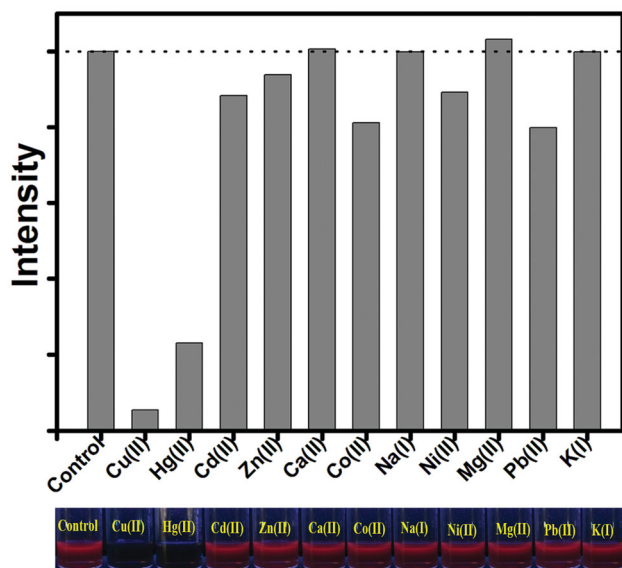

Figure 6. Upper panel: Selectivity of the HgS@BSA to different metal ions. The luminescence intensities are recorded at 730 nm. For all cases, the final metal ion concentrations are 50 ppm. Dotted line refers to see the change of luminescence with respect to the control one. Lower panel: Photographs of the HgS@BSA solution under UV light after addition of 50 ppm of various metal ions.

(Scheme 2) as in the protein environment Cu(II) is reduced to Cu(I).[31] In order to evaluate the sensing efficiency of the HgS QDs, we have added different concentrations of Hg(II) and Cu(II) to a fixed concentration (2 mg/mL) of QD solution (see Figure S11, SI). As shown in Figure S11, the luminescence of HgS QDs is reduced as a result of increasing either metal ion concentration. In order to unravel the consequence of the metallophilic interaction, a series of systematic picosecond-resolved photoluminescence studies were performed. The shorter excited-state lifetime of the HgS/Hg(II) and HgS/Cu(II) with respect to that of the free HgS QDs are clearly noticeable from **Figure 7**A,B. Details of the fitting parameters of the time-resolved decays are tabulated in **Table 1**. As evidenced from our study, the nature of the quenching of the QD lifetime by metal ions is dynamic.

There are two possible types of dynamic quenching mechanisms through which a metal ion center can induce the nonradiative deactivation of QD luminescence: electron transfer or energy transfer. As far as the electron-transfer mechanism is concerned, it can occur between species in intimate contact. Energy transfer, which involves deactivation of an electronic excited state of the donor and concomitant formation of an excited state of the acceptor, can occur via through-space (Förster) or through-bond (Dexter) mechanisms.[32] The Förster mechanism[33] requires direct donor–acceptor spectral overlap and arises from the Coulombic interaction between the donor and acceptor electric fields. However, in case of HgS-Cu(II)/HgS-Hg(II), the probability of such energy transfer is usually negligible due to the lack of absorption of the unsupported metal ions (Cu and Hg). Dexter transfer[34] is identical to the Förster mechanism but does not require significant oscillator strength on the part of the acceptor. It requires direct donor–acceptor orbital overlap; and has an exponential-distance dependence with a range of ~1 nm.

In the present study, both the possibilities, i.e., electron transfer or Dexter energy transfer can account for Hg(II) and Cu(II) inducing the lifetime quenching of the HgS QDs. To investigate the electron transfer dynamics from the HgS QDs upon excitation, we studied the complexation of the HgS QDs with an organic molecule, benzoquinone (BQ), which is well-known as an electron acceptor[35] and efficiently accepts excited electrons from the surface of semiconductor quantum dots.[36] As revealed from the inset of Figure 7B, in the presence of BQ a very sharp decay (monitored at 730 nm) is observed, which is associated with the transfer of excited electrons from the conduction band (CB) of the HgS QDs into the lowest unoccupied molecular orbital
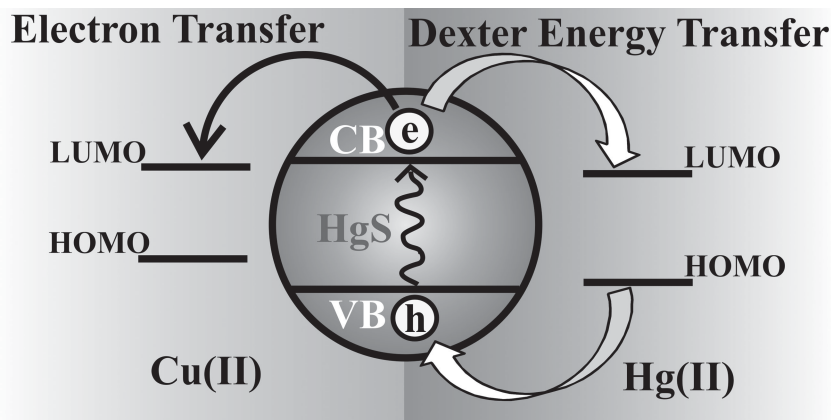
Scheme 2. Schematic representation of the excited-state quenching mechanism for the Cu(II) and Hg(II) ion. HOMO and VB represents highest occupied molecular orbital and valence band, respectively.

(LUMO) of the BQ molecules. It can be seen from Table 1 that the HgS/BQ system exhibits an ultrafast time component of 55 ps with a majority (86%) of the excited electrons following this path. The similar faster decay component, i.e., 30 ps (82%) in the presence of Cu(II) as compared to HgS/BQ system at the same excitation of 409 nm may be indicative of favorable electron transfer from the HgS QDs to the Cu(II) rather than Dexter energy transfer. However, the possibility of such an energy transfer cannot be completely ruled out.

After the addition of Hg(II) solution to the HgS@BSA, although the decay is faster compared to the HgS@BSA, no such ultrafast time constant with a majority like HgS/BQ system was found, which reveals the electron transfer is not associated with this process. Assuming the formation of a Hg(II)–Hg(II) metallophilic bond, the filled $5d_z^2$ and empty 6s orbital of each Hg(II) would overlap with each other,[37] which then give rise to bonding and anti-bonding orbitals.[38] Reorganization of these orbitals would therefore lead to new energy-accepting levels on the Hg(II), which provides the basis of a double electron exchange process (Dexter). We have also estimated the rate of energy transfer (k_{ET}) and energy transfer efficiency (E) by using the following equations:

$$k_{ET} = 1/\tau_q - 1/\tau_u \tag{1}$$

$$E = 1 - \tau_q/\tau_u \tag{2}$$

where τ_q is the "quenched" lifetime, here 1.5 ns; and τ_u is the "unquenched" lifetime, here 5 ns. From our time-resolved study, the rate of energy transfer (k_{ET}) and energy transfer efficiency (E) are found to be 4.7×10^8 s^{-1} and 72%, respectively.

Additionally, we performed DLS study to determine the effect of aggregation on the luminescence of as-prepared HgS@BSA. As shown in Figure S12 (SI), the addition of Hg(II) to the HgS@BSA solution has an insignificant effect
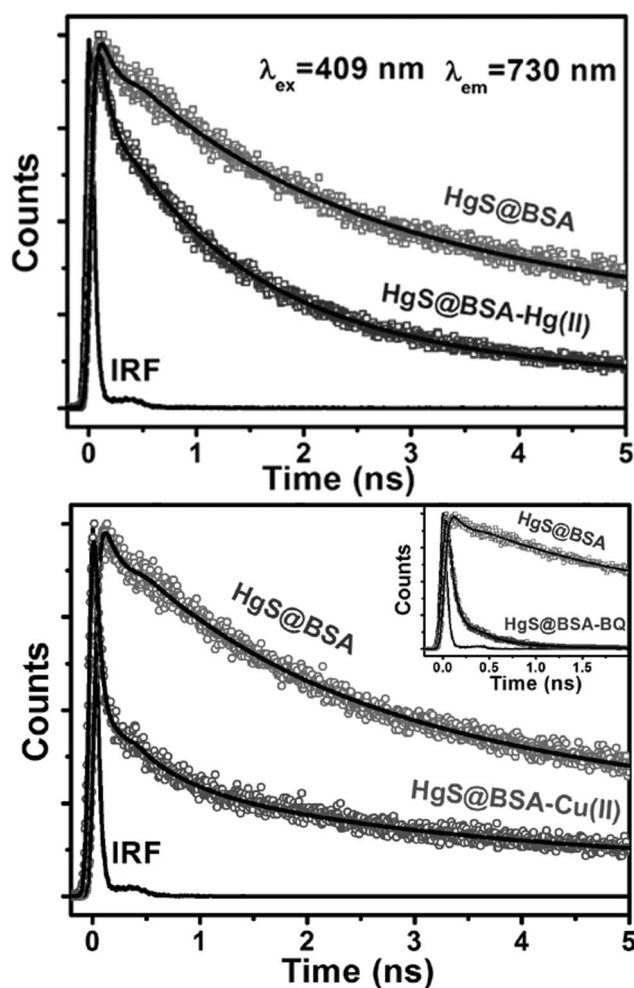

Figure 7. A) The picosecond time-resolved fluorescence transients of HgS QDs, in the absence and in the presence of acceptor Hg(II). B) The picosecond time-resolved fluorescence transients of HgS QDs, in the absence and in the presence of acceptor Cu(II). Inset showing the analogous data of HgS QDs, in the absence and in the presence of benzoquinone.

Table 1. Picosecond time-resolved luminescence transients of HgS@BSA in the absence and presence of Hg(II) and Cu(II). Lifetime values of the HgS@BSA system in presence of the well-known electron accepting agent, benzoquinone, is also shown. The luminescence of HgS QDs (maximum wavelength, $\lambda_{max} = 730$ nm) was detected with a 409 nm excitation laser. Numbers in parentheses indicate relative weightage.

System	τ_1 [ps]	τ_2 [ps]	τ_3 [ns]	τ_4 [ns]	τ_{av} [ns]
HgS@BSA	-	120(0.23)	1.8(0.40)	12.5(0.36)	5.2
HgS@BSA_Hg(II)	-	105(0.43)	1.2(0.42)	6.5(0.15)	1.5
HgS@BSA_Cu(II)	30(0.82)	430(0.07)	2.5(0.07)	17.0(0.04)	1.0
HgS@BSA_BQ	55(0.86)	320(0.12)	1.2(0.02)	-	0.1

on the size of HgS QDs, which rules out the possibility of luminescence quenching due to QDs aggregation.[16] In the case of HgS@BSA solution containing Cu(II), the DLS peak at ~9 nm remains unaltered; however, a new peak around 150 nm appeared which is consistent with the aggregation of the free protein in solution.[16] To further confirm the aggregation effect by Cu(II) and Hg(II), a control experiment was carried out with ethylenediaminetetraacetate (EDTA). EDTA can chelate both the metal ions in a 1:1 ratio and Cu(II) has more affinity towards EDTA than BSA.[39] If the metal ion induces the aggregation of the HgS@BSA, then, in the presence of EDTA, the metal ion would be chelated and should result in the recovery of its luminescence. However, no such recovery effect was observed even in a 1:2 (metal ion):EDTA ratio (data not shown), which further corroborates the direct interaction between the QDs with Cu(II) and Hg(II) ions. Attempts were also made to separate the metal ions from the protein-capped QDs by extensive dialysis against Milli-Q water. However, no evidence of the dissociation of the metal ions resulting the recovery of the QD luminescence was observed.

3. Conclusion

We have developed a simple straightforward bio-mineralization process for the synthesis of HgS QDs using a model protein, BSA. These QDs are extremely stable, luminescent-tunable from 685–800 nm, and highly quantum efficient. The luminescence of as-prepared QDs can be used for a highly sensitive and selective sensing system for the detection of Hg(II) and Cu(II). The sensing mechanism is demonstrated to be based on the formation of a metallophilic bond between Hg(II)/Cu(II) and Hg(II) present on the surface of the HgS QDs. In the excited state, the metallophilic bond facilitates the Dexter energy transfer to the Hg(II) and electron transfer to the Cu(II) over other processes associated with dynamic quenching. The synthetic approach and the metal-ion sensing with the proper mechanism described herein may be extended to other types of protein–semiconductor conjugates with tailored properties for diverse applications.

4. Experimental Section

Materials: BSA, sodium sulphide, $HgNO_3$ as well as the nitrates and chlorides of various metal ions were obtained from Sigma. The electron-accepting BQ was obtained from Alfa-Aesar. Milli-Q (from Millipore) water was used throughout the experiments. All the chemicals were used as received without further purification.

Synthesis of Protein-Stabilized HgS QDs: It involves two steps. In the first step, the nonluminescent HgO nanoparticles were prepared in a vial by dissolving 5 mL of 5 mM $HgNO_3$, H_2O, and 5 mL BSA (15 mg/mL) solution in MQ water under vigorous stirring with final pH value of ~9 (adjusted by 1 M NaOH solution carefully). Then, the solution was allowed to stir for 8–12 h. The final color of the solution was pale yellow, indicative to the formation of HgO@BSA nano-bioconjugates. In the second step, 4 mL of 20 mM Na_2S was added to 10 mL of as-synthesised HgO@BSA nano-bioconjugates, and

the solution was stirred for 15 min. Completion of the reaction was observed visibly by color changes from pale yellow to light brown. Such a color transition is indicative of the formation of HgS QDs.

Synthesis of Bulk HgO: Bulk HgO samples were prepared in a vial by dissolving 5 mL of 50 mM $HgNO_3$, H_2O, and 1 mL of 2.5 M NaOH solution. Then, the solution was allowed to stir for 15 min to obtain the yellow precipitate of HgO. Subsequently, the precipitate was centrifuged and washed with additional MQ water several times before measurements.

Synthesis of Bulk HgS: About 70 mg of $HgNO_3$, H_2O, and 70 mg Na_2S powder were dissolved in 5 mL MQ water under vigorous stirring. The reaction mixture was stirred for 30 min. The resulting precipitate was collected and repeatedly washed with MQ water by centrifugal precipitation. Finally, the bulk HgS precipitate was dried in an incubator to obtain a dark brown powder.

UV–Vis Absorption Spectroscopy: Optical absorption spectra of the solutions were measured with a Shimadzu spectrophotometer using a quartz cuvette of 1 cm path length. The experimentally obtained spectral data, $I(w)$, which are functions of wavelength, were converted to energy-dependent data, $I(E)$, according to the following relation,

$$I(E) = I(w)/(\delta E/\delta w) \, \alpha I(w) \times w^4 \tag{3}$$

where $\delta E/\delta w$ represents the Jacobian factor.

Photoluminescence (PL) Spectroscopy: The PL spectra were recorded on a Jobin Yvon Fluoromax-3 fluorometer.

DLS: DLS measurements were performed with Nano S Malvern instrument employing a 4 mW He-Ne laser (λ = 632.8 nm) equipped with a thermostated sample chamber. All the scattered photons are collected at 173° scattering angle. The scattering intensity data are processed using the instrumental software to obtain the hydrodynamic diameter (d_H) and the size distribution of the scatterer in each sample. The instrument measures the time-dependent fluctuation in the intensity of light scattered from the particles in solution at a fixed scattering angle. d_H of the proteins is estimated from the intensity autocorrelation function of the time-dependent fluctuation in intensity. d_H is defined as:

$$d_H = \frac{k_b T}{3\pi \eta D} \tag{4}$$

where k_b is the Boltzmann constant, T is the temperature, η is the viscosity, and D is the translational diffusion coefficient. In a typical size distribution graph from the DLS measurement, the X-axis shows a distribution of size classes in nanometers, while the Y-axis shows the relative intensity of the scattered light.

XPS: XPS measurements were conducted using an Omicron ESCA Probe spectrometer with unmonochromatized Al Kα X-rays (energy = 1486.6 eV). The X-ray power applied was 300 W. The pass energy was 50 eV for survey scans and 20 eV for specific regions. The base pressure of the instrument was 2.2×10^{-10} mB. The binding energy was calibrated with respect to the adventitious C 1s feature at 285.0 eV.

Raman Spectroscopy: Raman spectroscopic investigations were carried out using a confocal Raman microscope (CRM α300 S) purchased from WITec GmbH, Germany. The spectral acquisition was done in a back scattered geometry using a dispersion grating of 600 groves/mm. Detector was a peltier cooled charge coupled device which was maintained at −60 °C. The QDs were excited

with a HeNe 633 nm laser source. Each spectrum is an average of 100 hardware spectra, each of which is integrated over 1 s. Raman spectra were measured for BSA, HgO@BSA, and HgS@BSA in solid state, obtained after lyophilizing the corresponding solutions.

TEM: TEM images were taken using a FEI TecnaiTF-20 field-emission high-resolution transmission electron microscope operating at 200 kV. Samples for TEM imaging were prepared by placing a drop of as-prepared QDs solution on a carbon-coated Cu grid, and the solvent was evaporated under a bulb.

SEM: SEM images were taken using a FEG-SEM (FEI, Helios 600) operated at 20 kV.

Time-Correlated Single-Photon Counting: Picosecond-resolved fluorescence decay transients were measured by using a commercially available spectrophotometer (Life Spec-ps, Edinburgh Instruments, UK) with 60 ps instrument response function (IRF). The observed fluorescence transients were fitted using a nonlinear least-square fitting procedure to a function $(X(t) = \int_0^t E(t\prime) R(t - t\prime) dt\prime)$ comprising convolution of the IRF $(E(t))$ with a sum of exponential $(R(t) = A + \sum_{i=1}^N B_i e^{-t/\tau_i})$ with pre-exponential factors (B_i), characteristic lifetimes (τ_i) and a background (A). Relative concentration in a multiexponential decay was finally expressed as: $c_n = \frac{B_n}{\sum_{i=1}^N B_i} \times 100$. The quality of the curve fitting was evaluated by reduced chi-square and residual data. It has to be noted that with our time-resolved instrument, we can resolve at least one-fourth of the instrument response time constants after the de-convolution of the IRF.

CD Spectroscopy: The CD spectra were measured in a Jasco 815 spectropolarimeter with a Peltier setup for the temperature-dependent measurements. The cell path length was 10 mm.

FT-IR Spectroscopy: FT-IR spectra were measured with a Perkin Elmer Spectrum One instrument. KBr crystals were used as the matrix for sample preparation. Powder samples of BSA, HgO@BSA, and HgS@BSA (which were collected after lyophilization) were measured.

Quantum Yield Calculations: The quantum yield was calculated according to the following equation:[40]

$$Q = Q_R \left(\frac{I}{I_R} \right) \left(\frac{OD_R}{OD} \right) \left(\frac{n^2}{n_R^2} \right) \quad (5)$$

where Q and Q_R are the quantum yield of the protein and reference (DCM in methanol), I and I_R are the integrated fluorescence intensities of the protein and reference, OD and OD_R are the optical densities of the protein and reference at the excitation wavelength, and n and n_R are the refractive indices of the protein and reference solutions. The absolute quantum yield of DCM in methanol[41] was taken to be 0.43.

Supporting Information

Supporting Information is available from the Wiley Online Library or from the author.

Acknowledgements

[1] I. L. Medintz, M. H. Stewart, S. A. Trammell, K. Susumu, J. B. Delehanty, B. C. Mei, J. S. Melinger, J. B. Blanco-Canosa, P. E. Dawson, H. Mattoussi, *Nat. Mater.* **2010**, *9*, 676.
[2] L. Wu, B. Quan, Y. Liu, R. Song, Z. Tang, *ACS Nano* **2011**, *5*, 2224.
[3] M. K. So, C. J. Xu, A. M. Loening, S. S. Gambhir, J. H. Rao, *Nat. Biotechnol.* **2006**, *24*, 339.
[4] P. Yang, Y. Zhao, Y. Lu, Q. Z. Xu, X. W. Xu, L. Dong, S. H. Yu, *ACS Nano* **2011**, *5*, 2147.
[5] M. F. Frasco, N. Chaniotakis, *Sensors* **2009**, *9*, 7266.
[6] M. Razeghi, Y. Wei, A. Gin, G. J. Brown, *Mater. Res. Soc. Symp. Proc.* **2002**, *692*, 99.
[7] S. Keuleyan, E. Lhuillier, P. Guyot-Sionnest, *J. Am. Chem. Soc.* **2011**, *133*, 16422.
[8] W. Wichiansee, M. N. Nordin, M. Green, R. J. Curry, *J. Mater. Chem.* **2011**, *21*, 7331.
[9] K. A. Higginson, M. Kuno, J. Bonevich, S. B. Qadri, M. Yousuf, H. Mattoussi, *J. Phys. Chem. B* **2002**, *106*, 9982.
[10] Y. G. Yang, H. G. Liu, L. J. Chen, K. C. Chen, H. P. Ding, J. Hao, *Langmuir* **2010**, *26*, 14879.
[11] T. Ren, S. Xu, W. B. Zhao, J. J. Zhu, *J. Photochem. Photobiol. A* **2005**, *173*, 93.
[12] A. Mathew, P. R. Sajanlal, T. Pradeep, *J. Mater. Chem.* **2011**, *21*, 11205.
[13] J. P. Xie, Y. G. Zheng, J. Y. Ying, *Chem. Commun.* **2010**, *46*, 961.
[14] C. L. Guo, J. Irudayaraj, *Anal. Chem.* **2011**, *83*, 2883.
[15] S. S. Narayanan, S. K. Pal, *J. Phys. Chem. C* **2008**, *112*, 4874.
[16] N. Goswami, A. Giri, M. S. Bootharaju, P. L. Xavier, T. Pradeep, S. K. Pal, *Anal. Chem.* **2011**, *83*, 9676.
[17] A. V. Singh, B. M. Bandgar, M. Kasture, B. L. V. Prasad, M. Sastry, *J. Mater. Chem.* **2005**, *15*, 5115.
[18] P. L. Xavier, K. Chaudhari, A. Baksi, T. Pradeep, *Nano Reviews* **2012**, *3*, 14767.
[19] W. Zhou, F. Baneyx, *ACS Nano* **2011**, *5*, 8013.
[20] Y. Long, D. Jiang, X. Zhu, J. Wang, F. Zhou, *Anal. Chem.* **2009**, *81*, 2652.
[21] B. B. Campos, M. Algarra, B. Alonso, C. M. Casado, J. C. G. Esteves da Silva, *Analyst* **2009**, *134*, 2447.
[22] T. Zhou, U. Schwarz, M. Hanfland, Z. X. Liu, K. Syassen, M. Cardona, *Phys. Status Solidi b* **1996**, *198*, 411.
[23] S. V. Gotoshia, L. V. Gotoshia, *J. Phys. D: Appl. Phys* **2008**, *41*, 115406.
[24] B. A. Bolton, J. R. Scherer, *J. Phys. Chem.* **1989**, *93*, 7635.
[25] A. Dong, P. Huang, W. S. Caughey, *Biochemistry* **1990**, *29*, 3303.
[26] P. L. Xavier, K. Chaudhari, P. K. Verma, S. K. Pal, T. Pradeep, *Nanoscale* **2010**, *2*, 2769.
[27] L. Shang, Y. Wang, J. Jiang, S. Dong, *Langmuir* **2007**, *23*, 2714.
[28] P. Pyykko, *Angew. Chem. Int. Ed.* **2004**, *43*, 4412.
[29] S. Sculfort, P. Braunstein, *Chem. Soc. Rev.* **2011**, *40*, 2741.
[30] M. Kim, T. J. Taylor, F. P. Gabbai, *J. Am. Chem. Soc.* **2008**, *130*, 6332.
[31] K. J. Wiechelman, R. D. Braun, J. D. Fitzpatrick, *Anal. Biochem.* **1988**, *175*, 231.
[32] G. D. Scholes, K. P. Ghiggino, A. M. Oliver, M. N. Paddonrow, *J. Am. Chem. Soc.* **1993**, *115*, 4345.
[33] T. Forster, *Discuss. Faraday Soc.* **1959**, *27*, 7.
[34] D. L. Dexter, *J. Chem. Phys.* **1953**, *21*, 836.
[35] N. Goswami, A. Makhal, S. K. Pal, *J. Phys. Chem. B* **2010**, *114*, 15236.
[36] C. Burda, T. C. Green, S. Link, M. A. El-Sayed, *J. Phys. Chem. B* **1999**, *103*, 1783.

[37] A. Gorling, N. Rosch, D. E. Ellis, H. Schmidbaur, *Inorg. Chem.* **1991**, *30*, 3986.

[38] C.-K. Li, X.-X. Lu, K. M.-C. Wong, C.-L. Chan, N. Zhu, V. W.-W. Yam, *Inorg. Chem.* **2004**, *43*, 7421.

[39] M. A. H. Muhammed, P. K. Verma, S. K. Pal, A. Retnakumari, M. Koyakutty, S. Nair, T. Pradeep, *Chem. Eur. J.* **2010**, *16*, 10103.

[40] J. Chen, S. L. Flaugh, P. R. Callis, J. King, *Biochemistry* **2006**, *45*, 11552.

[41] H. Du, R.-C. A. Fuh, J. Li, L. A. Corkan, J. S. Lindsey, *Photochem. Photobiol.* **1998**, *68*, 141.